Reactive and Functional Polymers 208 (2025) 106164

Contents lists available at ScienceDirect

Reactive and Functional Polymers

journal homepage: www.elsevier.com/locate/react

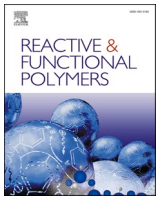

Digital light processing 3D printing of molecularly imprinted polymers for antibiotic removal

Elena Camilli [a], Valentina Bertana [b], Francesca Frascella [a], Matteo Cocuzza [a,b,c], Simone Luigi Marasso [b,c], Ignazio Roppolo [a,*]

[a] Department of Applied Science and Technology, Politecnico di Torino, C.So Duca Degli Abruzzi 24, Turin 10129, Italy
[b] Chilab - Materials and Microsystems Laboratory, Department of Applied Science and Technology, Politecnico di Torino, Via Lungo Piazza d'Armi 6, IT 10034, Chivasso, Turin, Italy
[c] Consiglio Nazionale delle Ricerche, Institute of Materials for Electronics and Magnetism (CNR-IMEM), Parco Area delle Scienze 37A, Parma 43124, Italy

ARTICLE INFO

Keywords:
Molecularly imprinted polymers
3D printing
Antibiotic removal
Digital light processing

ABSTRACT

Molecularly Imprinted Polymers (MIPs) as artificial receptors have received considerable scientific attention in the past few decades, as material for biomimetic molecular recognition. This paper explores the fabrication of MIPs by Additive Manufacturing (AM), which appears mostly as an unexplored field. Specifically Digital Light Processing (DLP) technology was employed to fabricate 3D-printed MIPs, imprinted with Oxytetracycline (OTC), a widespread antibiotic, whose presence in food and water must be controlled. The optimized MIP formulation also includes Methacrylic Acid as the functional monomer, Dipropylene Glycol Diacrylate as the crosslinker, and Dimethyl Sulfoxide as the solvent. The study demonstrates the recognition properties of the printed MIPs, showing enhanced binding performance with higher concentrations of the target molecule. The results underscore the potential of 3D-printed MIPs for a multitude of applications, including biomedical and environmental monitoring.

1. Introduction

Biological living systems have, during billions of years of evolution, developed an endless plethora of strategies to detect and respond to different internal and external stimuli, ensuring their adaptation to changing environmental conditions. The possible stimuli can be classified into two main categories: physical (such as electrical, mechanical, or light stimulation) and chemical [1]. In the latter, a prominent role is played by molecular recognition [2]. In this context, living species have optimized enzymes, antibodies and receptors to recognize molecules, as a fundamental scheme to guarantee their survival and proliferation. [3] With the development of bioengineering devices, science tried to replicate this strategy, striving to mimic the level of complexity of Nature in systems controllable by humans [4]. In this frame, biological receptors play paramount importance in biomedical and bioengineering devices, serving as elements capable of detecting and quantifying specific biological molecules in a wide range of applications [5]. The most conventional way to use these types of receptors is by employing them directly into the devices, as in standard Enzyme-Linked Immunosorbent Assay (ELISA), [6] as well as in biosensors, through surface interaction [7] and functionalization [8–10]. Still, these methods imply a series of drawbacks strictly related to the fragility of biological molecules [11].

Conversely, the approach of Molecular Imprinting has emerged as an innovative strategy. Indeed, Molecular Imprinting Technology (MIT) directly employs the molecules to be recognized as a template during the fabrication process to obtain a synthetic mould of the molecules, avoiding the intrinsic limitations of biological receptors [4,12]. In this context, since the 1970s [13], Molecularly Imprinted Polymers (MIPs) have been used as synthetic frameworks designed to have specific recognition sites for a determined target molecule. By MIT, a three-dimensional polymer matrix is synthesized in the presence of the molecule of interest, often referred to as the template molecule. Through the copolymerization of functional and crosslinking monomers, the template is thus incorporated into the network. Washing away the template, specific binding sites are left behind in the polymer, complementary in shape and functionality to the template. This introduces a form of memory into the polymer, enabling the molecular recognition and binding of target analytes [14].

* Corresponding author.
E-mail address: ignazio.roppolo@polito.it (I. Roppolo).

https://doi.org/10.1016/j.reactfunctpolym.2025.106164
Received 14 October 2024; Received in revised form 19 December 2024; Accepted 10 January 2025
Available online 12 January 2025

The advantages of MIPs encompass their physical and chemical robustness, making them well-suited for use in harsh environments. Their applications span diverse areas, including sensing [11,15], drug delivery [16–19], food and water analysis [20–22] and separation techniques [23–25]. However, MIPs are not exempt from challenges, including the complexity in the selection of ingredients and in optimizing the synthesis conditions [26]. Also, the efficient removal of the template molecule may be not a trivial process [27] and non-selective binding usually takes place to some extent [28].

Several techniques can be employed to fabricate MIPs, each with its own advantages and limitations, and the choice of the technique depends on the characteristics of the MIP, such as the nature of the template molecule or the intended application. The methods to synthesize the matrix around the template include electrochemical, thermal, photochemical or redox polymerization [29]. One of the first and most classic methods [30] implies the bulk polymerization of a volume of MIP, then sieved up to particles, usually not homogeneous in size and shape. To obtain more regular particles, over the years the techniques have been refined, and new methods have been adopted [4,28,31] such as emulsion [32], suspension [33] and precipitation polymerization [34], down to more recent multistep and complex procedures as surface imprinting [35] and core-shell nanoparticles [36]. Generally, the focus has been on spherical nanoparticles, to maximize the surface area, and thus the contact area with the target molecules. Moreover, techniques suitable for obtaining thin films and deposition on surfaces have been investigated [15,21] such as electrochemical deposition [37,38].

Despite many significant benefits, the use of nanoparticles or thin films also implies the limitation of not having self-supporting and arbitrary structures. A method that could provide such versatility is intuitively Additive Manufacturing (AM). Even though there are some studies on micro and nano-fabrication techniques [29,39,40], the use of AM for MIP fabrication is still quite an unexplored field. To the best of our knowledge, the pre-existing works are represented by L. P. Chia Gomez et al. [41] who fabricated 3D MIP microsensors by Two-Photon Stereolithography, and R. Rezanavaz et al. [42] who employed the Digital Light Processing (DLP) printer, to obtain MIP imprinted with copper ions. However, these studies are proofs of concept and didn't use the selective binding to target an actual biomolecule, limiting their investigation to ions and ad-hoc molecules. In this paper, the 3D printing of Molecularly Imprinted Polymers by Digital Light Processing was investigated, addressing the challenge of fabricating 3D, self-standing, and customizable objects imprinted with a molecule relevant to biomedical and environmental applications, specifically Oxytetracycline (OTC), a common antibiotic. DLP was chosen, as AM technique, because it is a reliable and straightforward technology. It is a vat polymerization (VP) technique, in which a vat filled with liquid formulation is selectively exposed to the light source, solidifying controlled layers of resin [43]. The object is built layer by layer on the printing platform, submerged in the liquid resin. DLP exploits a digital micromirror device, comprising thousands of tiny mirrors, to reflect the light source and project the pattern of each layer with high resolution. This technology, along with the quick conversion of the resin from liquid to solid achievable through the photopolymerization reaction, makes DLP suitable for the creation of flat vertical surfaces with minimal distortion and excellent shape accuracy [44]. This technology seems particularly useful for the development of complex MIPs. First, operating with liquid formulations, DLP allows a wide choice of functional monomers for the polymer network. Then, it allows direct mixing of the target molecule, without undergoing thermal stresses which may lead to its degradation. Finally, compared to other techniques, it enables higher complexity and higher resolution (down to features smaller than 100 μm), keeping at the same time a good printing rate and the possibility to fabricate macroscopic objects [45].

Oxytetracycline (OTC) was chosen as the template molecule. OTC is an antibiotic belonging to the tetracycline family and is a pervasive contaminant of soils and water, a consequence of the abuse of its utilization in modern zootechnics as well as in veterinary and human curative medicine [46]. Tetracyclines are indeed extensively employed in the livestock industry, and the administration to animals is the first step to a chain of events that not only causes pollution but also supports the issue of antibiotic resistance. MIPs offer a promising solution for the extraction of antibiotics from liquid samples [21,47,48]. The chosen target molecule is particularly relevant for food chain monitoring since the concentration of OTC should be strictly controlled in different matrices as milk, eggs, and honey [49–51]. To the best of our knowledge, this is the first time that this molecule is captured by a 3D-printed object with MIP resin. Moreover, for the first time, the possibility to fabricate macroscopic objects with recognition toward a target biological molecule is investigated. Also, the employment of an AM technique opens up to an extensive freedom in the design of the structure, and significant variability in terms of materials properties, contingent upon the selection of the precursors. In the fabrication of MIP, this flexibility is an appealing feature, keeping in mind that the optimization of the formulation and the printing parameters is the key to ensure an efficient imprinting process.

2. Results and discussion

The approach employed in this study for the development of 3D printable MIPs is sketched in Fig. 1, which illustrates the steps involved: preparation of suitable photocurable resins, 3D printing and then debinding/rebinding steps. So, the primary step of this study was to develop a formulation suitable for light-induced 3D printing with inherent recognition properties for a selected molecule of interest, while ensuring high-resolution outcomes during the printing process.

The design of MIP must take into account a series of elements, such as the choice of ingredients and their relative ratio [26,27,52], the presence of a solvent [53] and the rebinding conditions [54]. One of the most crucial aspects, though, is the choice of the functional monomer. The functional monomer must have a high capability of binding the template, in a covalent or non-covalent way, depending on the type of MIP. In the non-covalent ones, the functional monomer and the template must self-assemble, arranging in a pre-polymerization complex as stable as possible. A common monomer for MIP is Methacrylic acid (MAA), which, thanks to the carboxyl group, can form many types of interactions with different templates [55]. In this study, MAA is expected to self-arrange around the OTC, forming multiple hydrogen bonds with the amide and hydroxyl groups exposed by the OTC [49,53,56–58], as schematically depicted in Fig. 1.

For the purpose of developing a formulation compatible with both the molecular imprinting and the 3D printing processes, achieving a homogenous mixture is fundamental. This may need the inclusion of a solvent to facilitate the proper solubilization of the monomer and the template, thereby favouring their interaction in the generation of the pre-polymerization complex. In the current case, Dimethyl Sulfoxide (DMSO) was used to tackle the difficulty of solubilizing the antibiotic. Furthermore, it is essential to select a crosslinker appropriate both for the DLP printer and for the interaction with the functional monomer, so that it generates an accessible yet stable polymeric matrix. For this purpose, Dipropylene Glycol Diacrylate (DPGDA), a di-functional acrylate, was selected. This monomer was chosen over more traditional crosslinkers for MIP (such as ethylene glycol dimethacrylate - EGDMA [59]) due to the better performance in 3D printing. In fact, unlike more rigid crosslinkers, like EGDMA, DPGDA did not show cracking due to shrinkage stresses after 3D printing, keeping a good balance between the ability to form the cavity structures and the maintenance of sufficient swellability and flexibility to allow solvent permeation during the binding and debinding steps. In summary, the optimized MIP formulation comprised: Oxytetracycline as the template, Methacrylic acid as the functional monomer, Dipropylene Glycol Diacrylate as the crosslinker, and DSMO as the solvent. As the photoinitiator, Phenylbis(2,4,6-trimethylbenzoyl)phosphine oxide (BAPO) was used. The same

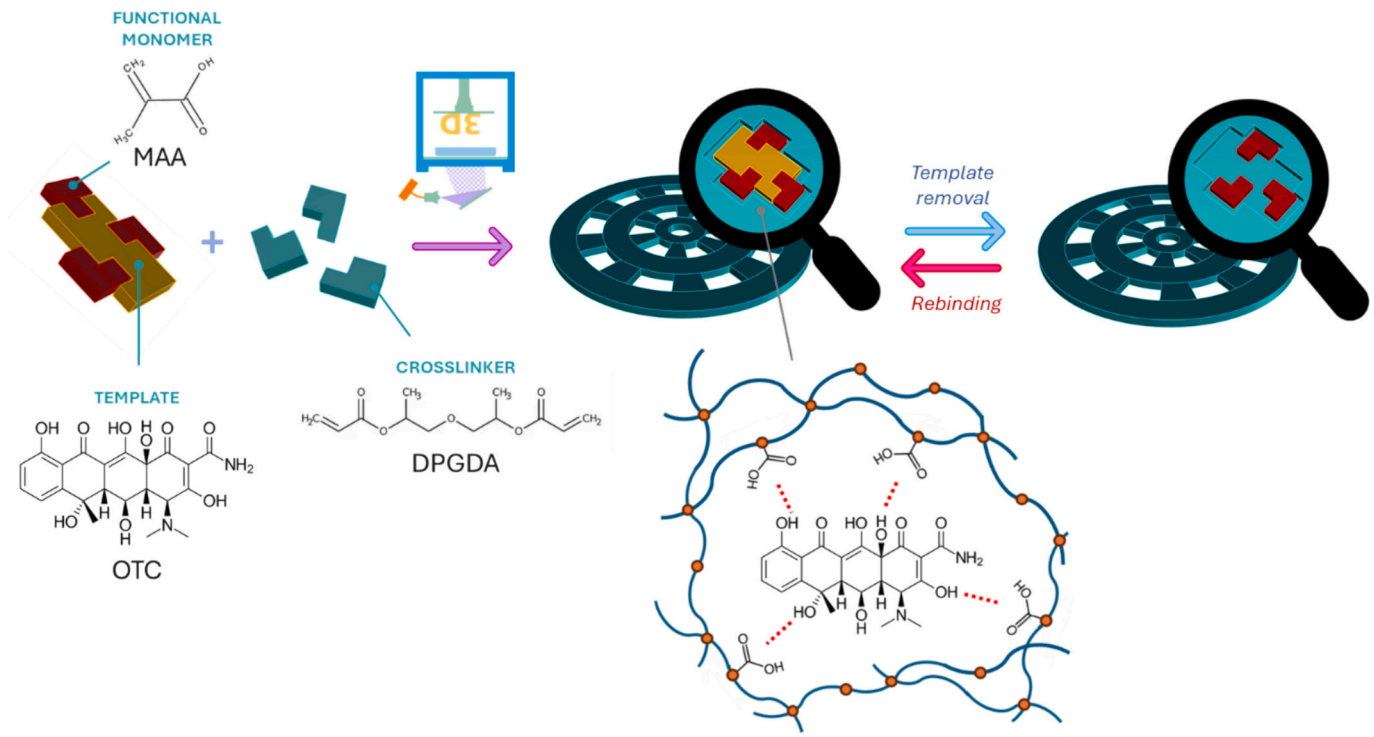

Fig. 1. A sketched representation of the 3D-printed molecularly imprinted polymer fabrication process.

procedure was employed for the preparation of Non-Imprinted Polymers (NIPs), except for adding the template. NIPs serve as control elements to distinguish the efficacy of the molecular imprinting from the unspecific affinity of the monomers with the template. Details are reported in the method section.

Once the formulation was prepared, preliminary tests on printability were conducted. Firstly, the viscosities of both MIP and NIP formulations were determined through rheological measurements, to investigate any potential impact of the antibiotic on this property, crucial for light-induced 3D printing. The results revealed a comparable behaviour between the two resins, as shown in Fig. 2(a), and viscosity values are deemed suitable for DLP processing [60]. Secondly, real-time photorheology was employed to evaluate the effect of the antibiotic in the MIP resin on the polymerization kinetic. As shown in Fig. 2(b), the presence of the target molecule plays a threefold role during photopolymerization. First, the beginning of the polymerization is delayed: while the NIP formulation reacts almost immediately, the MIP shows a delay time of about 20 s. Then, during the first 10 s of polymerization, the slope of the MIP curve is 99 % less steep compared to that of the NIP curve, indicating that the MIP formulation has slower reaction kinetics. At last, the value of storage modulus G' plateau decreases in the formulation with the target molecule. This can be related to crosslinking density due to a hindering effect of OTC, but also to a decrease of secondary forces (such as H-bonds) in the network, with MMA carboxylic group bonded to OTC instead of establishing bonds with ester moieties in the polymeric network. The slower polymerization kinetics can be attributed to the absorbance of the antibiotic within the range of irradiation of the printer (385 nm), as can be seen in the UV–Vis spectrum in Fig. S1. Thus, the antibiotic competes with the photoinitiator in the absorbance of light, acting essentially as a dye [61].

The UV–Visible absorbance spectra of both the formulation and a thin printed layer were examined. This analysis aimed to evaluate the stability of the antibiotic following photopolymerization, confirming that the component associated with the presence of OTC in the formulation remains intact after the printing process. As illustrated in Fig. 2(c), the spectrum of the MIP formulation exhibits a characteristic tail that persists in the spectrum of the printed MIP, and that significantly differs from the NIP spectra.

Noteworthy, photorheology indicates the behaviour of the formulations, nevertheless, optimum printing parameters should be found directly through testing with the actual equipment. The first printed objects were multi-material disks consisting of a base made of DPGDA, 500 μm thick, with a 50 μm thick layer of MIP/NIP resin on top (Fig. 3 (a)). The diameter of the disks is 10 mm. The thickness of the MIP/NIP layer was minimized to have a thin active coating on a surface, mimicking a functionalization film. Through iterative experiments, the optimal printing parameters in terms of time of light exposure, light intensity and layer thickness, were found (Table S1). Consistent with the photorheological characterization, the MIP resin needed a longer time and a higher power to polymerize, compared to the NIP resin. The presence of the OTC allowed to achieve a better confinement of the polymerization process in the xy plane and lower light penetration on the z-axis. So, despite the relatively long printing time, the silver lining lies in the possibility of printing high-resolution objects with the MIP formulation [61].

Fourier-transform infrared (FT-IR) spectroscopy in attenuated total reflectance (ATR) was conducted both before and after resin polymerization (Fig. S2) to assess the conversion of the C═C double bonds to C—C single bonds, thereby evaluating the reaction of acrylic groups in DPGDA, and of methacrylic ones in MAA. For both MIP and NIP, the formulations achieved a 70 % acrylate conversion rate. The calculations are reported in Table S2. Although not exceptionally high, this degree of conversion is deemed suitable for 3D printing applications [62]. Additionally, the spectra of the MIP/NIP formulations and printed samples were compared to that obtained directly from the Oxytetracycline powder. As depicted in Fig. 2(d), a distinct peak at 1580 cm^{-1} in the OTC spectrum is present in the MIP formulation and, even if weaker, is recognizable also in the spectra of the printed polymer. Meanwhile, this peak is absent in NIP. This observation confirms the presence of the antibiotic on the surface of the 3D-printed MIP. Upon successful fabrication of the multi-material disks, the binding capability of the novel material must be assessed. As described in reference studies [56,58], the

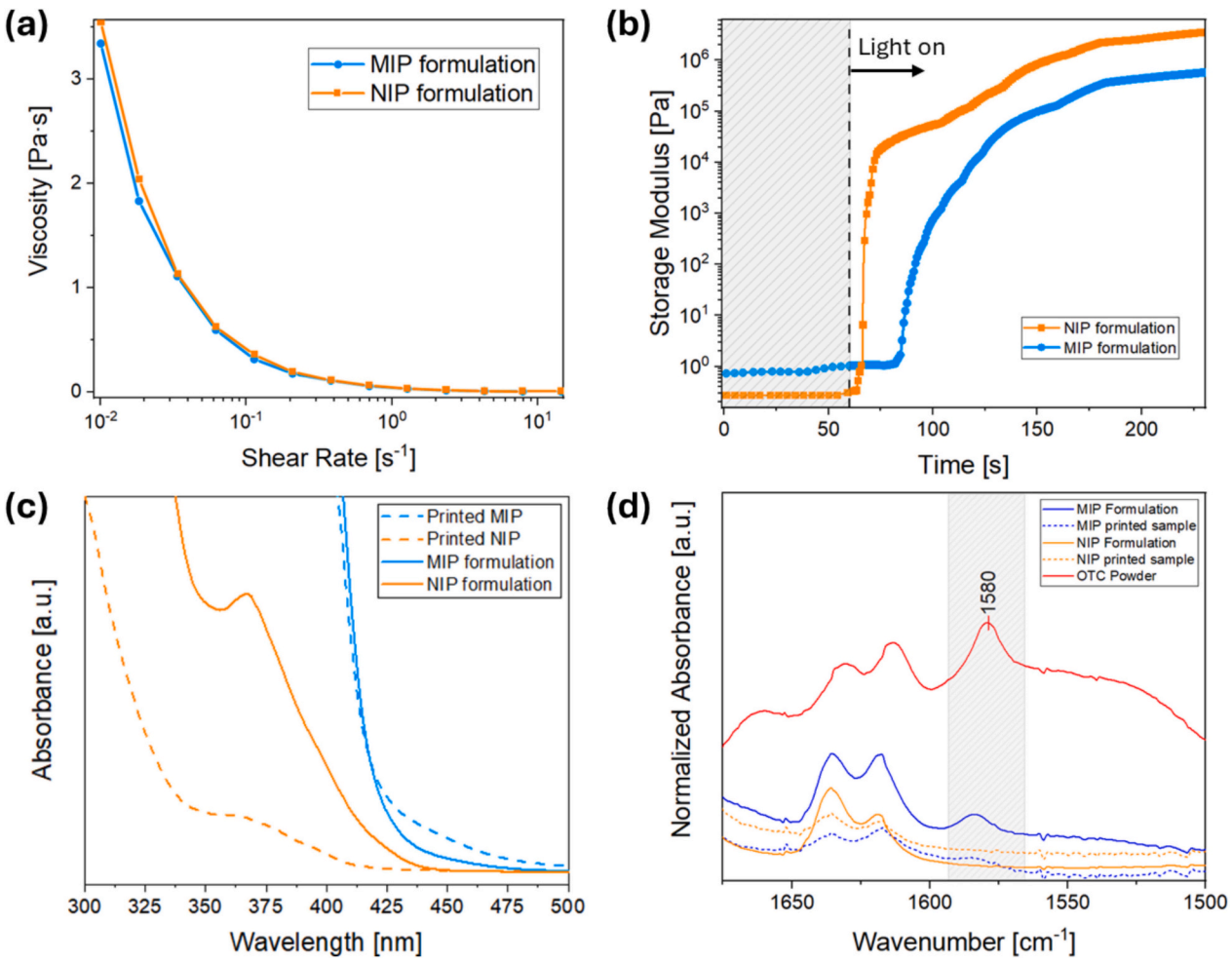

Fig. 2. (a) Viscosity of MIP and NIP formulations under continuous shear rate sweep. (b) Real-time photorheological measure of the MIP and NIP formulations. (c) UV–visible spectra of formulations and thin printed samples, both of MIP and NIP, showing the presence of a yellow component only in the MIP due to the presence of the OTC. (d) ATR FT-IR spectra of both liquid formulations and printed samples, and the pure antibiotic in powder. (For interpretation of the references to colour in this figure legend, the reader is referred to the web version of this article.)

sample underwent rebinding testing using different concentrations of the binding solution (C_S), specifically 50 μM, 75 μM, 100 μM and 150 μM of OTC in deionized water, to compare the binding ability in the presence of a different amount of target. Water was chosen as solvent given the intended application in water purification. The percent of removed target and the Imprinting Factor (IF) obtained from the experiments are detailed in Table 1. Under identical experimental conditions, the most effective binding performances were observed at the highest target concentration. Specifically, the removal percentage reaches the highest value in the case of 150 μM solution, with nearly 14 % of the target bound to the MIPs from the initial solution. This result is almost twice that of the 75 μM solution and respectively 54 % and 70 % higher than the 50 μM and 100 μM.

In all cases, a portion of non-specific binding occurs, evident from the non-negligible binding of NIPs. It should be noted that in molecular imprinting techniques the non-specific binding is often inevitable and generally arises from the inherent affinity of the target to the functional monomer, that provides functionalities independently from the presence of imprinted cavities [48].

Notably, for the 50 μM, 75 μM, and 100 μM solutions, the behaviour of both the imprinted and non-imprinted samples exhibited substantial similarity (Fig. 6(a)). However, with an increase in target concentration, the disparity between the two became more pronounced, as indicated by the Imprinting Factor (IF) reaching its peak with the 150 μM solution (Table 1). This behaviour may suggest that the differences in binding performance between the MIP and NIP may not be as pronounced due to the limited number of interactions at low concentrations. This indicates that higher concentrations could magnify these differences, allowing the rebinding with the MIP to become more evident.

Moreover, it is noticed that at the higher concentration the binding values for the NIP are comparable to the binding observed for both MIP and NIP at lower concentrations. This suggests that the non-specific binding component remains relatively constant across all conditions, while the contribution of specific binding increases with target concentration, enhancing the differentiation between MIP and NIP. The structural composition of the multi-material disks may be a factor of the aforementioned outcomes: part of the nonspecific interaction can be attributed to the presence of the "base" layer of the disk. This underlying layer lacks molecular imprinting specificity and contributes to the observed background binding. Indeed, the structural differentiation between the MIP and NIP disks is confined to the 50 μm thick "active" layer, where the imprinted sites are located. These considerations suggest the elimination of such non-functional components in the next designs, to increase the binding site differentiation and increase the specific rebinding capacity of MIP systems. Nevertheless, at the present stage this was necessary for fabrication limitations.

Before fabricating more complex shapes, the printed materials were characterized in terms of thermal properties and morphology. Thermogravimetric (TGA) experiments and the derivate of this signal (DTG) showed that after washing step MIP and NIP samples have the same

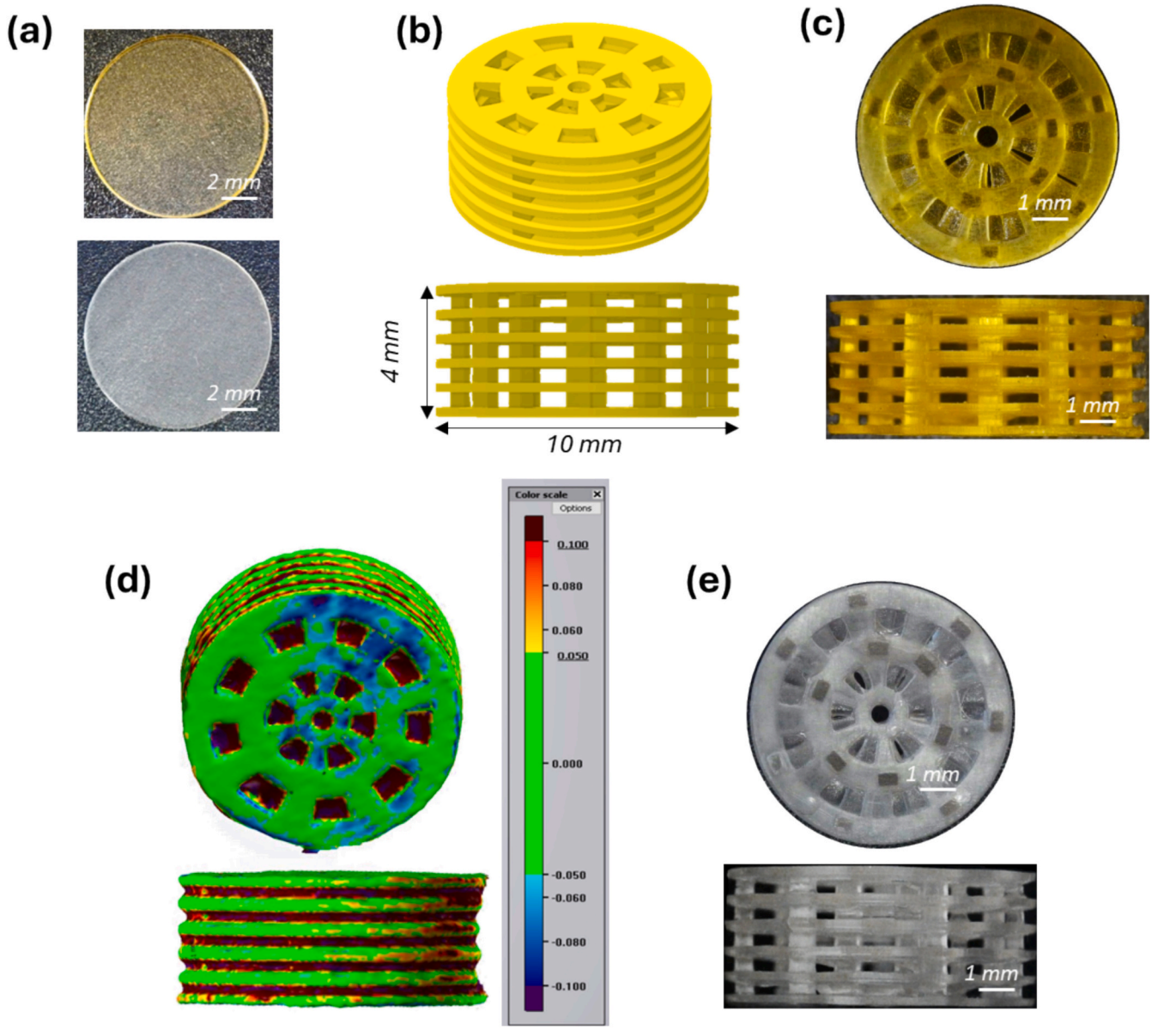

Fig. 3. (a) Image of MIP (top) and NIP (bottom) printed disks. (b) CAD of the MIP filter. (c) Image of the related printed object and (d) its 3D scan. (e) Image of the MIP filter after the washing procedure that removed the template from the polymeric matrix.

Table 1
Comparison between MIP and NIP performances with different concentrations of the rebinding solutions.

C_s (μM)		%Removal	IF
50	MIP	9.00 ± 2.0	1.2
	NIP	7.46 ± 0.4	
75	MIP	7.46 ± 1.6	0.8
	NIP	9.07 ± 2.9	
100	MIP	8.15 ± 0.9	0.8
	NIP	9.4 ± 1.7	
150	MIP	13.9 ± 3.3	1.6
	NIP	8.6 ± 3.6	

degradation mechanism, with two main degradation steps around 370 °C and 380 °C (Figs. 4(a) and 4(b)). This is consistent with ATR experiments and indicates the successful removal of OTC. On the contrary MIP and NIP samples have clear differences, especially for degradation mechanism at low temperatures (Fig. 4(c)): while NIP sample presents a first degradation step between 120 °C and 210 °C, which can be related to DMSO evaporation, MIP sample show a shift toward higher temperatures, that can be associated to OTC degradation, as previously reported [63]. Both NIP and MIP are in the glassy state at room temperature, being the glass transition temperatures (T_g) above 75 °C for both, as reported in Supporting Information File (Fig. S3, Table S3 and DSC comments). This results in stiff objects easy to handle. Considering that the envisaged application does not require strong mechanical requirements, in this case mechanical properties were not considered, nevertheless this aspect will be treated in next investigations. After the washing step all the materials maintained similar properties, demonstrating that washing step is effective for the removal of the antibiotic without damaging the structure. Unfortunately, repeated binding/washing cycles lead to stresses and damaging of the structures, as shown in Fig. S4, which at the present stage limits the reusability of these 3D printed materials. This aspect is also under investigation for enhancements.

The effect of the washing step was then investigated by scanning electronic microscopy (SEM). In Fig. 5 micrographs of the surface of NIP

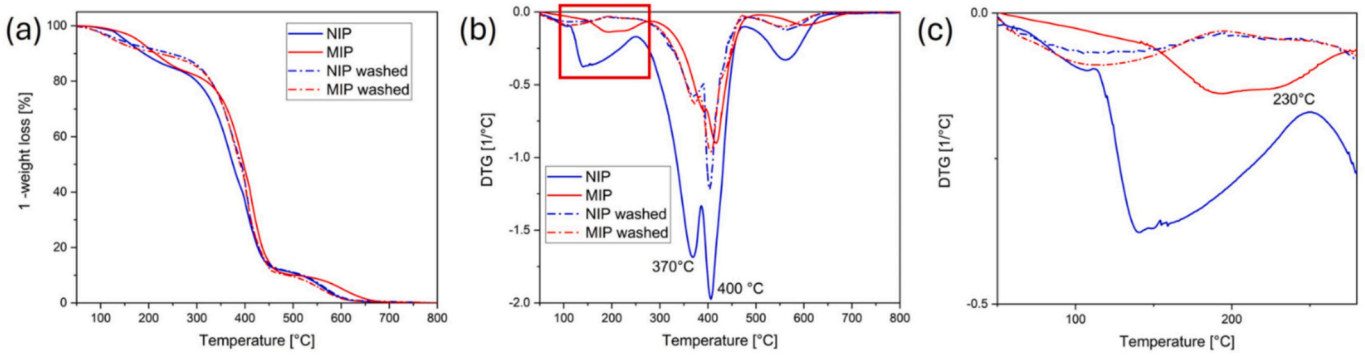

Fig. 4. (a) TGA curves of NIP and MIP samples as printed and after washing step. (b) First derivative of TGA (DTG). (c) Magnification of DTG between 50 °C and 270 °C.

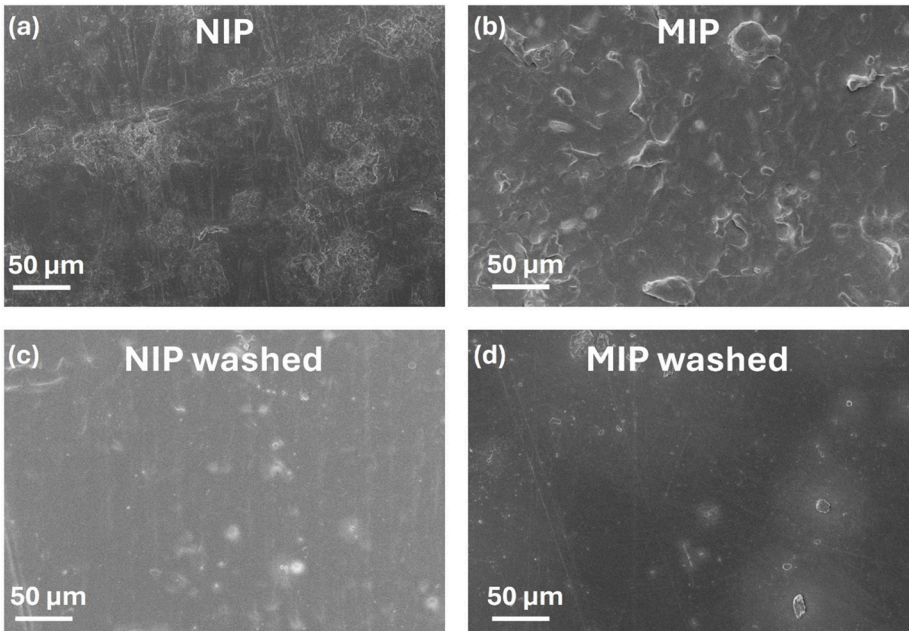

Fig. 5. SEM surface pictures of (a) NIP and (b) MIP samples after 3D printing, and (c) NIP and (d) MIP samples after the washing step.

and MIP samples were reported, both before and after the washing step. As expected, after 3D printing both NIP and MIP surfaces appear similar, since the only difference between the two formulations is in the presence of OTC, which has sub-nm dimension and cannot be observed by SEM. After the washing step both the surfaces seem smoother, but without cracks, indicating that some modification may occur in the polymer rearrangements, but without dramatically affecting the integrity of the sample.

Having assessed the effect of the washing step on a flat disk, more complex, all-MIP objects were fabricated. In the context of this work, the most captivating aspect of 3D printing is the possibility of creating complex and customizable objects. This implies the potential of building elaborate designs with high surface area, thus enhancing the accessibility to the imprinted cavities. To showcase this versatility, within the scope of developing MIPs for antibiotic recovery from water, a filter-shaped, micro-structured MIP has been 3D printed as proof of concept (Fig. 3(c)).

The MIP formulation performed nicely, allowing to print high-resolution objects, being the achieved finest feature 200 µm on the xy plane. The accuracy of the printed MIP-objects with respect to the CAD (Fig. 3(b)) was measured by a 3D scanner (Fig. 3(d)). The results showed an excellent fidelity to the design, with discrepancies within ±50 µm. Larger deviations are related to the impossibility of the scanner to accurately measure internal cavities. Despite the small features, the 3D-printed filters showed good structural resistance, maintaining the integrity of the polymeric matrix after the washing procedure and the elimination of the template (Fig. 3(e)).

Considering the aforementioned results, the filter-shaped MIPs were tested under the most favourable binding condition of 150 µM solution of OTC. The results were encouraging: the MIPs removed from the 32.5 % OTC solution (Table 2). As anticipated, the filters outperformed the flat disks in terms of removal percentage. The enhanced binding observed is attributed to the higher surface area and the intricate geometry, which allows a more extensive interaction with the surrounding solution containing the target. Also, the Binding Capacity (BC) was calculated, showing that the filter bound 90 µg of OTC per each g of polymer.

In this case, instead of having a non-imprinted counterpart, three different filter-shaped MIPs were tested also in a solution containing a

Table 2
Binding performances of filter-shaped MIP.

C_s (µM)	*Analyte*	*%Removal*	*BC* ($\mu g\ g^{-1}$)
150	OTC	32.5 ± 2.1	93.7 ± 6.2
	SDMO	14.7 ± 5.3	42.9 ± 15.5

different analyte, namely Sulfadimethoxine (SDMO). SDMO is another antibiotic commonly found as a contaminant in aquatic environments [64], and it was chosen to assess the material's ability to distinguish between the target molecule (OTC) and structurally different compounds, providing insights into the imprinting selectivity of the MIPs. The filters were incubated in a solution containing 150 μM of SDMO. The spectral analysis showed that the removal of SDMO was less than half of the binding of the equivalent samples with the OTC, as shown in Fig. 6 (b) and Table 2. This suggests that the OTC-imprinted polymer exhibits a significantly higher affinity for binding with the imprinted molecule compared to others. Such results could signify another promising characteristic of the investigated MIP. On the other hand, a more in-depth study is required to validate these outcomes and to be applied in real operating devices, which will be carried out in future investigations, while this report aimed at focusing on the development and validation of the production process.

To sum up, this experiment validates the material's capability to collect the target molecule from the aqueous solution. It is important to notice that the performances are quite limited compared to the well-established techniques that usually involve MIP in nanoparticles, which for the removal of OTC may reach over 80 % of removal and binding capacity in the order of mg g^{-1} [49,53,56–58]. However, a direct comparison with established studies on nanoparticles MIPs would be inherently biased, as nanoparticles typically exhibit significantly higher surface area, and thus higher site accessibility and faster mass transfer compared to the bulkier, macroscopic polymers presented here. On the other hand, the few existing studies on 3D-printed MIPs have substantial differences in terms of template molecules and polymer compositions [41,42]. Nonetheless, the binding capacity observed in this work is in line with the results reported in such studies, consistently with the novelty of the fabrication technique.

3. Conclusions

In this manuscript, the possibility of merging the properties of MIP with the versatility of Rapid Prototyping was investigated to freely generate objects with molecular recognition capability. A MIP photopolymerizable resin compatible with Digital Light Projection technology was successfully developed. The selection of the proper precursors allowed obtaining molecular imprinting properties meanwhile achieving the 3D printing of high-resolution objects. The successful removal of OTC in aqueous solutions indicates potential applications in environmental analysis and water treatment. Noteworthy, this is the first study that reports on the development of 3D printed MIPs for similar applications.

Even if the overall removal of the target is lower compared to the well-established approach of MIPs in the form of particles, the results here reported allow for the use of macroscopic objects, which can be used as filters, integrated as solid elements in larger systems or as parts of fluidic devices. Further investigations shall enhance the imprinting efficiency, thereby increasing the Imprinting Factor and improving the Binding Capacity of the MIPs. This could involve optimizing the ratio of the resin components or exploring alternative geometries to maximize the surface area of the printed structures. Furthermore, mechanical properties will be better developed in next studies, to improve reusability of such devices. On the other hand, the findings here reported clearly indicates the interesting opportunities that the exploration of the applicability of 3D-printed MIPs can give in real-world scenarios for the selective recovery of antibiotics from complex media.

4. Experimental section

4.1. Materials

Oxytetracycline hydrochloride, methacrylic acid, Phenylbis(2,4,6-trimethylbenzoyl)phosphine oxide (BAPO), dimethyl sulfoxide and Sulfadimethoxine were purchased from Merck (Milan, Italy). Dipropylene Glycol Diacrylate was purchased by Allnex.

4.2. Formulation preparation

The photocurable ink was prepared by mixing the oxytetracycline and the methacrylic acid. In the literature, the molar ratios employed for MIP formulation vary significantly even with the same template and functional monomers, reflecting diverse approaches to optimize MIP's fabrication. In this work, the chosen molar ratio was inspired by the recommendations from reference studies [26], along with the consideration that OTC has a limited number of functional groups available for interactions. Thus, the template-to-functional-monomer ratio of 1:4 was adopted [57]. The addition of a solvent was deemed necessary due to the difficulty of dispersing the OTC, and the minimum quantity of dimethyl sulfoxide (DMSO) required for a clear pre-polymerization complex solution was determined to be 10.6 % wt. The solution underwent stirring for one hour at room temperature. Separately, BAPO (0.8 % of crosslinker) was added to the DPGDA (template: crosslinker ratio set at 1:20), and dissolved with the help of an ultrasound bath.

The two solutions were then combined and thoroughly mixed until achieving homogeneity, as verified by the transparency of the

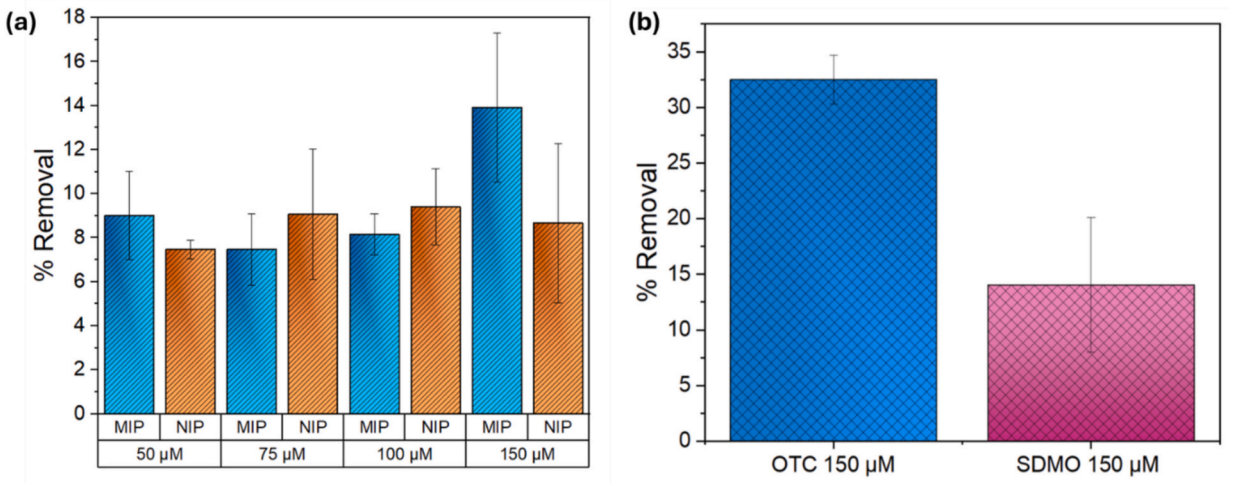

Fig. 6. %Removal of (a) MIP and NIP disks, with different concentrations solutions of the target molecule, and (b) OTC-imprinted filters in 150 μM solutions of OTC or SDMO. Data are means of triplicate measurements.

formulation. At this point, the photocurable MIP formulation was obtained. For the Non-Imprinted Polymers (NIPs) formulation, the OTC was excluded.

4.3. Formulation characterization

Viscosities of both MIP and NIP formulations were evaluated through rheological measurements by the Anton Paar Physica MCR 302 rheometer, in a 25 mm diameter parallel plate mode, with a gap of 0.2 mm between plates and constant temperature of 25 °C. The rotation shear ramp test was performed between 0.01 s^{-1} and 1000 s^{-1}. To evaluate the effect of the antibiotic on the kinetic of the photopolymerization, real-time photorheology measures were performed. OTC absorbs in the range of exposure of the DLP, competing with the photoinitiator in the absorbance of light. The formulations with the antibiotic (MIP resin) and without the antibiotic (NIP resin) were compared. Photorheology of the two formulations was performed with the Anton Paar MCR 302 rheometer in plate-plate configuration. The light source was a Hamamatsu Photonics C8 UV lamp, with a light intensity of 50 mW cm^{-2}. The real-time photorheology was performed with a quartz bottom plate, temperature set to 25 °C, and with 1 % strain amplitude and angular velocity of 10 rad s^{-1}. After the stabilization time (60 s), the light was turned on and the change in the viscoelastic properties of the material during polymerization was measured over time. UV–visible spectra of both resin and printed object were collected to compare MIP and NIP, using the BioTek Synergy HTX Multi-Mode Microplate Reader (Agilent), in the range 250–450 nm. Moreover, Fourier Transform Infrared (FT-IR) spectroscopy was conducted on the liquid formulations and printed samples. Thermo Fisher Scientific Nicolet™ iS50 Spectrometer was used, in attenuated total reflectance (ATR) mode, in the range of 4000–550 cm^{-1}. The degree of conversion was determined by calculating the area at the peak corresponding to the C═C bond (1638 cm^{-1}) before and after polymerization. The quantification of the peak areas was carried out with Omnic™ Software (Thermo Fisher Scientific) after the normalization at the peak of the C═O bond at 1720 cm^{-1}, as it remains unaffected by the polymerization process. The spectra are reported in Fig. S2. Thermogravimetric analysis (TGA) was performed using a Netzsch TG 209 F1 Libra instrument in the range between 25 and 800 °C, with a heating rate of 10 °C min^{-1} in air atmosphere (flux 50 mL min^{-1}). The first derivative of TGA (DTG) was employed to evidence degradation mechanisms. Differential scanning calorimetry (DSC) measurements were performed with a Netzsch DSC 204 F1 Phoenix instrument, equipped with a low temperature probe. All the tests were performed in nitrogen atmosphere with the following thermal method: between 20 °C and 200 °C with a heating rate of 10 °C min^{-1}, 10 min isothermal at 200 °C, cooling cycle 200 °C–20 °C with a cooling rate of 10 °C min^{-1}, 15 min at 20 °C, second heating cycle between 20 °C and 200 °C with a heating rate of 10 °C min^{-1}. The Tg was defined as the midpoint of the heat capacity change observed in the DSC thermogram and calculated with Proteus software. The morphology of the dots was investigated by a Zeiss Supra 40 FESEM, equipped with a GEMINI II column and EDS analyzer, where a probe current of 1200 pA and an accelerating voltage between 5.00 and 15.00 kV were used. Magnification reported 250×.

4.4. 3D printing and 3D scanning

The Asiga MAX X UV 27 DLP printer was employed, with a LED light irradiation at 385 nm. The CAD models were designed with Solidworks software and then uploaded in *.stl* format in the proprietary printer software (Asiga Composer). The diameter of all the objects was 10 mm, to fit the samples inside the wells of a 48-multi-well plate, in which the different stages of the experiment take place. Layer thickness, light intensity, and exposure time depend on the formulation (MIP/NIP) and the geometry of the object. For the MIP formulation, the printing process was operated with a 25 or 50 μm layer thickness, a light intensity of 48 mW cm^{-2}, and an exposure time of 30 s. For the NIP formulation, the light intensity was decreased to 20 mW cm^{-2}, and the exposure time to 4.5/5 s. In Table S1 the detailed printing parameters are illustrated. The accuracy of the printed objects to the CAD model was evaluated by the 3Shape E3 scanner, whose acquisition was compared to the CAD models by a proprietary scanner software to obtain the deviation map. After printing, the samples undergo two post-polymerization steps. First, they are washed in ethanol to remove any unpolymerized resin, and then post-cured in a UV chamber (Asiga Flash) for 120 s to finalize the polymerization.

4.5. Washing process and rebinding

To remove the template within the polymer matrix, the samples go through a washing procedure using a solution of methanol and acetic acid (9,1 *v*/v). The samples are immersed in the washing solution and then placed in an ultrasound bath or on a tilting platform for several hours, depending on their volume. The intensity of the ultrasound bath was kept as low as possible, so to avoid significant damage to the samples, as it is possible to see in Fig. 3(e). During the washing process, the washing solution was iteratively replaced, and its UV–vis spectra were analysed to monitor the progress of template removal. The washing procedure was deemed complete when the spectra no longer displayed the characteristic OTC peak at 355 nm, and the spectrum of the washing solution of the sample is overlapped with clean methanol/acetic acid. An example is displayed in Fig. S5. Additionally, a visual indicator is the colour change in both the samples (previously yellow due to the presence of the OTC, they become more transparent as the antibiotic is washed away) and the washing solutions (turning from transparent to pale yellow). To ensure comparability, NIP samples underwent the same washing protocol as the MIPs, despite not containing a template molecule, to have a reliable control. The FT-IR spectra of the samples as printed and after washing were analysed to determine the removal of DMSO during the washing procedure (Fig. S6).

After the washing process that emptied the binding cavities, the samples were ready to interact with the solution containing the target molecule. Thus, the batch rebinding takes place, meaning the MIPs fully immersed in a solution of deionized water and OTC. Four different concentrations were prepared: 50 μM, 75 μM, 100 μM and 150 μM. The samples were placed in a well of a 48-well plate, immersed in 500 μL of the designated binding solution and left overnight on a tilting platform.

4.6. Evaluation of the binding properties

To assess the binding ability of the samples, UV–visible spectra of aliquots of the binding solutions were acquired both before and after exposure to the polymer, allowing a comparative analysis. Specifically, spectrophotometry was performed using the BioTek Synergy HTX Multi-Mode Microplate Reader (Agilent), in the range 250–450 nm, 1 nm intervals, and a UV–Vis-NIR Spectrophotometer Cary 5000 (Varian, Agilent) was used, range 200–450 nm, 1 nm intervals. After the acquisition of a calibration curve of the OTC (displayed in Fig. S7), the absorbance values were translated into concentrations, and the binding performances were evaluated. In Fig. S8 the spectra collected in all the experiments are depicted.

Several parameters can be calculated to characterize the binding performances of MIP. [26,49] The extent of the interaction between the polymer and the target molecule was described in terms of the percentage of OTC removed from the rebinding solution. The removal percentage is calculated using the formula:

$$\%\text{Removal} = \frac{C_s - C_f}{C_s} \times 100$$

Where C_s is the initial concentration of OTC in the solution, and C_f is the amount of free OTC in the solution after the incubation with the polymer. When possible, the Imprinting Factor (IF) was calculated as the

ratio between the removal percentage of imprinted and non-imprinted polymer:

$$IF = \frac{\%Removal_{MIP}}{\%Removal_{NIP}}$$

The IF reflects the effectiveness of the imprinting process, meaning how much the inherent affinity of the polymer to the template increases due to the presence of the imprinted cavities. Another useful figure of merit is the Binding Capacity (BC), namely the amount of bound OTC divided by the weight of the MIP.

Funding

This work was supported by the National Plan for Complementary Investments to the NRRP, project "D34H—Digital Driven Diagnostics, prognostics and therapeutics for sustainable Health care" (project code: PNC0000001), Spoke 4 funded by the Italian Ministry of University and Research.

CRediT authorship contribution statement

Elena Camilli: Writing – original draft, Investigation. **Valentina Bertana:** Writing – review & editing, Investigation. **Francesca Frascella:** Writing – review & editing, Supervision, Investigation. **Matteo Cocuzza:** Writing – review & editing, Resources. **Simone Luigi Marasso:** Writing – review & editing, Supervision. **Ignazio Roppolo:** Writing – original draft, Supervision, Methodology, Conceptualization.

Declaration of competing interest

The authors declare that they have no known competing financial interests or personal relationships that could have appeared to influence the work reported in this paper.

Appendix A. Supplementary data

Supplementary data to this article can be found online at https://doi.org/10.1016/j.reactfunctpolym.2025.106164.

Data availability

Data are reported either in the manuscript or in Supporting Information File

References

[1] P.S. Agutter, D.N. Wheatley, About Life: Concepts in Modern Biology, 1st ed., Springer, Dordrecht, 2007 https://doi.org/10.1007/978-1-4020-5418-1.
[2] E. Persch, O. Dumele, F. Diederich, Molecular recognition in chemical and biological systems, Angew. Chem. Int. Ed. (2015) 3290–3327, https://doi.org/10.1002/anie.201408487.
[3] P.C. Mariju, J. Navarro, From molecular recognition to the " vehicles " of evolutionary complexity : an informational approach, Int. J. Mol. Sci. 22 (2021) 11965, https://doi.org/10.3390/ijms222111965.
[4] O.I. Parisi, F. Francomano, M. Dattilo, F. Patitucci, S. Prete, F. Amone, F. Puoci, The evolution of molecular recognition: from antibodies to molecularly imprinted polymers (MIPs) as artificial counterpart, J. Funct. Biomater. 13 (2022), https://doi.org/10.3390/jfb13010012.
[5] J. Manhas, H.I. Eldestein, J.N. Leonard, L. Morsut, The evolution of synthetic receptor systems, Nat. Chem. Biol. 18 (2022) 244–255, https://doi.org/10.1038/s41589-021-00926-z.
[6] R.M. Lequin, Enzyme Immunoassay (EIA)/ Enzyme-Linked Immunosorbent Assay (ELISA) 2418, 2005, pp. 2415–2418, https://doi.org/10.1373/clinchem.2005.051532.
[7] L. Lunelli, F. Barbaresco, G. Scordo, C. Potrich, L. Vanzetti, S.L. Marasso, M. Cocuzza, C.F. Pirri, C. Pederzolli, PDMS-based microdevices for the capture of MicroRNA biomarkers, Appl. Sci. 10 (2020), https://doi.org/10.3390/app10113867.
[8] M. Barra, G. Tomaiuolo, V.R. Villella, S. Esposito, A. Liboà, P. D'Angelo, S. L. Marasso, M. Cocuzza, V. Bertana, E. Camilli, V. Preziosi, Organic electrochemical transistor Immuno-sensors for spike protein early detection, Biosensors 13 (2023), https://doi.org/10.3390/bios13070739.
[9] V. Preziosi, M. Barra, V.R. Villella, S. Esposito, P. D'Angelo, S.L. Marasso, M. Cocuzza, A. Cassinese, S. Guido, Immuno-sensing at ultra-low concentration of TG2 protein by organic electrochemical transistors, Biosensors 13 (2023), https://doi.org/10.3390/bios13040448.
[10] M. Segantini, M. Parmeggiani, A. Ballesio, G. Palmara, F. Frascella, S.L. Marasso, M. Cocuzza, Design of a portable microfluidic platform for EGOT-based in liquid biosensing, Sensors 22 (2022) 1–15, https://doi.org/10.3390/s22030969.
[11] M.J. Whitcombe, I. Chianella, L. Larcombe, S.A. Piletsky, J. Noble, R. Porter, A. Horgan, The rational development of molecularly imprinted polymer-based sensors for protein detection, Chem. Soc. Rev. 40 (2011) 1547–1571, https://doi.org/10.1039/c0cs00049c.
[12] L. Ye, K. Mosbach, Molecular Imprinting: Synthetic Materials as Substitutes for Biological Antibodies and Receptors, 2008, pp. 859–868.
[13] G. Wulff, A. Sahran, The use of polymers with enzyme-analogous structures for the resolution of racemates, Angew. Chem. Int. Ed. Eng. 46 (1972) 334–342, https://doi.org/10.1002/anie.197203341.
[14] M. Díaz-Álvarez, E. Turiel, A. Martín-Esteban, Recent advances and future trends in molecularly imprinted polymers-based sample preparation, J. Sep. Sci. 46 (2023), https://doi.org/10.1002/jssc.202300157.
[15] A.-M. Gavrilă, E.-B. Stoica, T.-V. Iordache, A. Sârbu, Modern and dedicated methods for producing molecularly imprinted polymer layers in sensing applications, Appl. Sci. 12 (2022) 3080, https://doi.org/10.3390/app12063080.
[16] A.E. Bodoki, B. Iacob, E. Bodoki, Perspectives of Molecularly Imprinted Polymer-Based Drug Delivery Systems in Cancer Therapy, 2019.
[17] F. Puoci, G. Cirillo, M. Curcio, O.I. Parisi, F. Iemma, N. Picci, Molecularly imprinted polymers in drug delivery: state of art and future perspectives, Expert Opin. Drug Deliv. 8 (2011) 1379–1393, https://doi.org/10.1517/17425247.2011.609166.
[18] R. Liu, A. Poma, Advances in molecularly imprinted polymers as drug delivery systems, Molecules 26 (2021), https://doi.org/10.3390/molecules26123589.
[19] S. He, L. Zhang, S. Bai, H. Yang, Z. Cui, X. Zhang, Y. Li, Advances of molecularly imprinted polymers (MIP) and the application in drug delivery, Eur. Polym. J. 143 (2021) 110179, https://doi.org/10.1016/j.eurpolymj.2020.110179.
[20] J. Meléndez-Marmolejo, L. Díaz de León-Martínez, V. Galván-Romero, S. Villarreal-Lucio, R. Ocampo-Pérez, N.A. Medellín-Castillo, E. Padilla-Ortega, I. Rodríguez-Torres, R. Flores-Ramírez, Design and application of molecularly imprinted polymers for adsorption and environmental assessment of anti-inflammatory drugs in wastewater samples, Environ. Sci. Pollut. Res. 29 (2022) 45885–45902, https://doi.org/10.1007/s11356-022-19130-0.
[21] H.Y. Hijazi, C.S. Bottaro, Molecularly imprinted polymer thin-film as a micro-extraction adsorbent for selective determination of trace concentrations of polycyclic aromatic sulfur heterocycles in seawater, J. Chromatogr. A 1617 (2020) 460824, https://doi.org/10.1016/j.chroma.2019.460824.
[22] H. Birtane, E. Kök, O. Ayd, B. Çi, Selective molecularly imprinted polymer for the analysis of chlorpyrifos in water samples 87 (2020) 145–151, https://doi.org/10.1016/j.jiec.2020.03.025.
[23] R. Oliveira, F. Mauro, A. Tim, R. Chaves, Analytica chimica acta molecularly imprinted polymers in online extraction liquid chromatography methods: current advances and recent applications 1284, 2023, https://doi.org/10.1016/j.aca.2023.341952.
[24] Z. Song, J. Li, W. Lu, B. Li, G. Yang, Y. Bi, M. Arabi, X. Wang, J. Ma, L. Chen, Molecularly imprinted polymers based materials and their applications in chromatographic and electrophoretic separations, Trends Anal. Chem. 146 (2022), https://doi.org/10.1016/j.trac.2021.116504.
[25] A. Azizi, C.S. Bottaro, A critical review of molecularly imprinted polymers for the analysis of organic pollutants in environmental water samples, J. Chromatogr. A 1614 (2020) 460603, https://doi.org/10.1016/j.chroma.2019.460603.
[26] D.A. Spivak, Optimization, evaluation, and characterization of molecularly imprinted polymers, Adv. Drug Deliv. Rev. 57 (2005) 1779–1794, https://doi.org/10.1016/j.addr.2005.07.012.
[27] M. Mabrouk, S.F. Hammad, A.A. Abdella, F.R. Mansour, Tips and tricks for successful preparation of molecularly imprinted polymers for analytical applications: a critical review, Microchem. J. 193 (2023) 109152, https://doi.org/10.1016/j.microc.2023.109152.
[28] D. Refaat, M.G. Aggour, A.A. Farghali, R. Mahajan, J.G. Wiklander, I.A. Nicholls, S. A. Piletsky, Strategies for molecular imprinting and the evolution of MIP nanoparticles as plastic antibodies — synthesis and applications, Int. J. Mol. Sci. 20 (2019) 6304, https://doi.org/10.3390/ijms20246304.
[29] E. Paruli, O. Soppera, K. Haupt, C. Gonzato, Photopolymerization and Photostructuring of molecularly imprinted polymers, ACS Appl. Polym. Mater. 3 (2021) 4769–4790, https://doi.org/10.1021/acsapm.1c00661.
[30] R. Arshady, K. Mosbach, Synthesis of substrate-selective polymers by host-guest polymerization, Makromol. Chem. 182 (1981) 687–692.
[31] F. Yemiş, P. Alkan, B. Yenigül, M. Yenigül, Molecularly imprinted polymers and their synthesis by different methods, Polym. Polym. Omposites 21 (2013) 145–150, https://doi.org/10.1177/096739111302100304.
[32] G. Zhao, J. Liu, M. Liu, X. Han, Y. Peng, X. Tian, Synthesis of molecularly imprinted polymer via emulsion polymerization for application in Solanesol separation, Appl. Sci. 10 (2020) 2068, https://doi.org/10.3390/app10082868.
[33] E.N. Ndunda, B. Mizaikoff, Synthesis of stationary phases that provide group recognition for polychlorinated biphenyls by porogenic fragment template imprinting, J. Sep. Sci. 39 (2016) 939–946, https://doi.org/10.1002/jssc.201500960.
[34] R.M. Roland, S.A. Bhawani, M.N.M. Ibrahim, Synthesis of molecularly imprinted polymer by precipitation polymerization for the removal of ametryn, BMC Chem. (2023) 1–20, https://doi.org/10.1186/s13065-023-01084-0.

[35] C. Dong, H. Shi, Y. Han, Y. Yang, R. Wang, J. Men, Molecularly imprinted polymers by the surface imprinting technique, Eur. Polym. J. 145 (2021) 110231, https://doi.org/10.1016/j.eurpolymj.2020.110231.
[36] L. Wan, Z. Chen, C. Huang, X. Shen, Core-shell molecularly imprinted particles, Trends Anal. Chem. 95 (2017) 110–121, https://doi.org/10.1016/j.trac.2017.08.010.
[37] S. Ramanavičius, I. Morkvėnaitė-vilkončienė, U. Samukaitė-bubnienė, V. Ratautaitė, I. Plikusienė, R. Viter, A. Ramanavičius, Electrochemically deposited molecularly imprinted polymer-based sensors, Sensors 22 (2022), https://doi.org/10.3390/s22031282.
[38] Y. Sasaki, Y. Zhang, H. Fan, K. Ohshiro, Q. Zhou, W. Tang, X. Lyu, T. Minami, Accurate cortisol detection in human saliva by an extended-gate-type organic transistor functionalized with a molecularly imprinted polymer, Sensors Actuators B Chem. 382 (2023) 1–10, https://doi.org/10.1016/j.snb.2023.133458.
[39] P.G. Conrad, P.T. Nishimura, D. Aherne, B.J. Schwartz, D. Wu, N. Fang, X. Zhang, M.J. Roberts, K.J. Shea, Functional molecularly imprinted polymer microstructures fabricated using microstereolithography, Adv. Mater. 15 (2003) 1541–1544, https://doi.org/10.1002/adma.200304602.
[40] A.V. Linares, A. Falcimaigne-Cordin, L.A. Gheber, K. Haupt, Patterning nanostructured, synthetic, polymeric receptors by simultaneous projection photolithography, nanomolding, and molecular imprinting, Small 7 (2011) 2318–2325, https://doi.org/10.1002/smll.201100248.
[41] L.P.C. Gomez, A. Spangenberg, X.A. Ton, Y. Fuchs, F. Bokeloh, J.P. Malval, B. Tse Sum Bui, D. Thuau, C. Ayela, K. Haupt, O. Soppera, Rapid prototyping of chemical microsensors based on molecularly imprinted polymers synthesized by two-photon Stereolithography, Adv. Mater. 28 (2016) 5931–5937, https://doi.org/10.1002/adma.201600218.
[42] R. Rezanavaz, M. Petcu, M.-J. Le Guen, A. Dubois, Three-dimensional printing of molecularly imprinted polymers by digital light processing for copper ion sequestration, 3D print, Addit. Manuf. (2022), https://doi.org/10.1089/3dp.2022.0107.
[43] A. Salas, M. Zanatta, V. Sans, I. Roppolo, Chemistry in light-induced 3D printing, ChemTexts 9 (2023) 1–16, https://doi.org/10.1007/s40828-022-00176-z.
[44] M. Caprioli, I. Roppolo, A. Chiappone, L. Larush, C.F. Pirri, S. Magdassi, 3D-printed self-healing hydrogels via digital light processing, Nat. Commun. 12 (2021) 1–10, https://doi.org/10.1038/s41467-021-22802-z.
[45] G. Gonzalez, I. Roppolo, C.F. Pirri, A. Chiappone, Current and emerging trends in polymeric 3D printed microfluidic devices, Addit. Manuf. 55 (2022) 102867, https://doi.org/10.1016/j.addma.2022.102867.
[46] P. Grenni, V. Ancona, A. Barra Caracciolo, Ecological effects of antibiotics on natural ecosystems: a review, Microchem. J. 136 (2018) 25–39, https://doi.org/10.1016/j.microc.2017.02.006.
[47] A.G. Ayankojo, J. Reut, V.B.C. Nguyen, R. Boroznjak, V. Syritski, Advances in detection of antibiotic pollutants in aqueous media using molecular imprinting technique—a review, Biosensors 12 (2022), https://doi.org/10.3390/bios12070441.
[48] R. Rodríguez-Dorado, A.M. Carro, I. Chianella, K. Karim, A. Concheiro, R. A. Lorenzo, S. Piletsky, C. Alvarez-Lorenzo, Oxytetracycline recovery from aqueous media using computationally designed molecularly imprinted polymers, Anal. Bioanal. Chem. 408 (2016) 6845–6856, https://doi.org/10.1007/s00216-016-9811-6.
[49] J.F.F. Aguilar, J.M. Miranda, J.A. Rodriguez, M.E. Paez-Hernandez, I.S. Ibarra, Selective removal of tetracycline residue in milk samples using a molecularly imprinted polymer, J. Polym. Res. 27 (2020), https://doi.org/10.1007/s10965-020-02139-9.
[50] Y.K. Lv, J.Q. Zhang, Z.Y. Guo, W. Zhang, H.W. Sun, Determination of tetracyclines residues in egg, milk, and milk powder by online coupling of a precolumn packed with molecular imprinted hybrid composite materials to RP-HPLC-UV, J. Liq. Chromatogr. Relat. Technol. 38 (2015) 1–7, https://doi.org/10.1080/10826076.2013.873873.
[51] B.D. Abera, I. Ortiz-gómez, B. Shkodra, F.J. Romero, G. Cantarella, L. Petti, A. Salinas-castillo, P. Lugli, A. Rivadeneyra, Laser-induced graphene electrodes modified with a molecularly imprinted polymer for detection of tetracycline in milk and meat, Sensors 22 (2022) 1–17, https://doi.org/10.3390/s22010269.
[52] T. Sajini, B. Mathew, A brief overview of molecularly imprinted polymers: highlighting computational design, nano and photo-responsive imprinting, Talanta Open 4 (2021) 100072, https://doi.org/10.1016/j.talo.2021.100072.
[53] M.P. Divya, Y.S. Rajput, R. Sharma, Synthesis and application of tetracycline imprinted polymer, Anal. Lett. 43 (2010) 919–928, https://doi.org/10.1080/00032710903491039.
[54] A.D. Khatibi, A.H. Mahvi, N. Mengelizadeh, D. Balarak, Adsorption–desorption of tetracycline onto molecularly imprinted polymer: isotherm, kinetics, and thermodynamics studies, Desalin. Water Treat. 230 (2021) 240–251, https://doi.org/10.5004/dwt.2021.27396.
[55] K. Nishchaya, V.K. Rai, H. Bansode, Methacrylic acid as a potential monomer for molecular imprinting: a review of recent advances, Results Mater. 18 (2023) 100379, https://doi.org/10.1016/j.rinma.2023.100379.
[56] W. Cai, R.B. Gupta, Molecularly-imprinted polymers selective for tetracycline binding, Sep. Purif. Technol. 35 (2004) 215–221, https://doi.org/10.1016/S1383-5866(03)00143-6.
[57] R. Suedee, T. Srichana, T. Chuchome, U. Kongmark, Use of molecularly imprinted polymers from a mixture of tetracycline and its degradation products to produce affinity membranes for the removal of tetracycline from water, J. Chromatogr. B 811 (2004) 191–200, https://doi.org/10.1016/j.jchromb.2004.08.044.
[58] M. Sánchez-Polo, I. Velo-Gala, J.J. López-Peñalver, J. Rivera-Utrilla, Molecular imprinted polymer to remove tetracycline from aqueous solutions, Microporous Mesoporous Mater. 203 (2015) 32–40, https://doi.org/10.1016/j.micromeso.2014.10.022.
[59] A. Adumitrăchioaie, M. Tertiş, A. Cernat, R. Săndulescu, C. Cristea, Electrochemical methods based on molecularly imprinted polymers for drug detection. A review, Int. J. Electrochem. Sci. 13 (2018) 2556–2576, https://doi.org/10.20964/2018.03.75.
[60] J.W. Stansbury, M.J. Idacavage, 3D printing with polymers: challenges among expanding options and opportunities, Dent. Mater. 32 (2016) 54–64, https://doi.org/10.1016/j.dental.2015.09.018.
[61] M. Gastaldi, F. Cardano, M. Zanetti, G. Viscardi, C. Barolo, S. Bordiga, S. Magdassi, A. Fin, I. Roppolo, Functional Dyes in Polymeric 3D Printing, 2021, https://doi.org/10.1021/acsmaterialslett.0c00455.
[62] G. Gonzalez, A. Chiappone, K. Dietliker, C.F. Pirri, I. Roppolo, Fabrication and functionalization of 3D printed polydimethylsiloxane-based microfluidic devices obtained through digital light processing, Adv. Mater. Technol. 5 (2020) 1–10, https://doi.org/10.1002/admt.202000374.
[63] P. Cervini, B. Ambrozini, L.C.M. Machado, A.P.G. Ferreira, E.T.G. Cavalheiro, Thermal behavior and decomposition of oxytetracycline hydrochloride thermal behavior and decomposition of oxytetracycline hydrochloride, J. Therm. Anal. Calorim. (2015), https://doi.org/10.1007/s10973-015-4447-x.
[64] L.A. Tom, N.A. Schneck, C. Walter, Improving the imprinting effect by optimizing template:monomer:cross-linker ratios in a molecularly imprinted polymer for sulfadimethoxine, J. Chromatogr. B Anal. Technol. Biomed. Life Sci. 909 (2012) 61–64, https://doi.org/10.1016/j.jchromb.2012.10.020.